Materials & Design 224 (2022) 111416

Contents lists available at ScienceDirect

Materials & Design

journal homepage: www.elsevier.com/locate/matdes

Ring inserts as a useful strategy to prepare tip-loaded microneedles for long-acting drug delivery with application in HIV pre-exposure prophylaxis

Alejandro J. Paredes [a], Andi Dian Permana [b], Fabiana Volpe-Zanutto [a], Muhammad Nur Amir [c], Lalitkumar K. Vora [a], Ismaiel A. Tekko [a], Nima Akhavein [d], Andrew D. Weber [e], Eneko Larrañeta [a], Ryan F. Donnelly [a,*]

[a] School of Pharmacy, Queen's University Belfast, 97 Lisburn Road, Belfast BT9 7BL, United Kingdom
[b] Department of Pharmaceutics, Faculty of Pharmacy, Hasanuddin University, Makassar, Indonesia
[c] Department of Pharmacology and Toxicology, Faculty of Pharmacy, Hasanuddin University, Makassar, Indonesia
[d] ViiV Healthcare, 1250 South Collegeville Rd, College, USA
[e] ViiV Healthcare, 410 Blackwell Street, Durham, NC 27701, USA

HIGHLIGHTS

- The use of MAPs for drug delivery has gained considerable attention over the last decade.
- MAPs can deliver drugs systemically for weeks, which is desirable in HIV PrEP.
- The manufacture of MAPs is associated with several challenges, including bubble formation.
- The ring inserts developed here allowed the formation of highly uniform MAPs.
- Long-acting delivery of CAB in rats was maintained for 14 days.

GRAPHICAL ABSTRACT

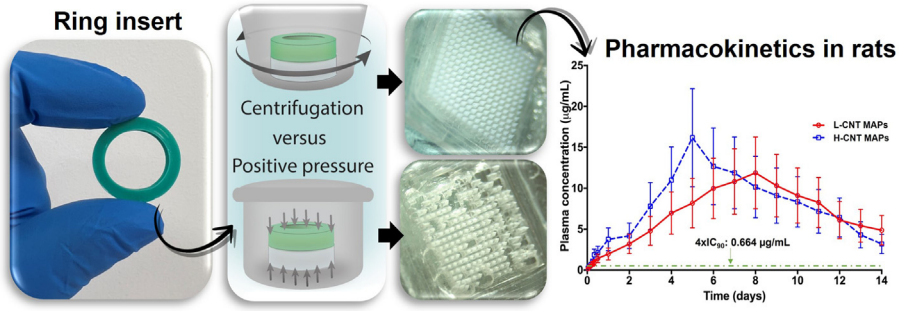

ARTICLE INFO

Article history:
Received 5 August 2022
Revised 14 November 2022
Accepted 21 November 2022
Available online 24 November 2022

Keywords:
Ring inserts
Dissolving microneedles
Cabotegravir sodium
Long-acting
Human immunodeficiency virus
Pre-exposure prophylaxis

ABSTRACT

The role of microneedle array patches (MAPs) and, in particular, dissolving MAPs in transdermal drug delivery has increased exponentially over the last decade. MAPs are able to form drug depots in the viable skin from where poorly soluble drugs dissolve in a long-acting fashion, showing promise in the management of multiple diseases. The manufacture of these systems can present some challenges, including the presence of bubbles in the baseplates and consequent lack of uniformity in microneedle formation and drug content. Here, we present a simple method based on ring inserts to produce tip-loaded MAPs using the antiretroviral drug cabotegravir sodium (CAB). The obtained MAPs presented a high uniformity in terms of microneedle formation, and a suitable insertion capability, as per the mechanical characterisation performed. An optimisation based on design of experiments revealed that centrifugation parameters had a significant impact on the skin deposition of the MAPs in excised neonatal porcine skin using Franz cells, with values ranging from 62.24 ± 47.13 μg to 174.13 ± 41.10 μg of CAB. Pharmacokinetic studies

Abbreviations: ACN, Acetonitrile; ARV, Antiretroviral; CAB, Cabotegravir sodium; CNT, Centrifuge; DoE, Design of experiments; HIV, Human immunodeficiency virus; HPLC, High performance liquid chromatography; H-CNT-MAPs, Microarray patches obtained at high centrifugation force; L-CNT-MAPs, Microarray patches obtained at low centrifugation force; MAPs, Microarray patches; MRT, Mean retention time; MNs, Microneedles; OCT, Optical coherence tomography; PC, Pressure chamber; PLA, Poly(lactic acid); PBS, Phosphate buffered saline; PreP, Pre-exposure prophylaxis; PVP, Poly(vinylpyrrolidone); PVA, Poly(vinyl alcohol).

* Corresponding author at: School of Pharmacy, Queen's University Belfast, 97 Lisburn Road, Belfast BT9 7BL, United Kingdom.
E-mail address: r.donnelly@qub.ac.uk (R.F. Donnelly).

https://doi.org/10.1016/j.matdes.2022.111416

carried out in rats evidenced the capacity of the MAPs to maintain therapeutic plasma levels of CAB for 14 days, with T_{max} values reached between 5 and 8 days.

1. Introduction

The use of microneedle array patches (MAPs) for patient monitoring purposes and the delivery of a wide variety of drugs has grown exponentially over the last decade [1]. In particular, dissolving MAPs have been proven to be one of the most versatile platforms for drug delivery through the skin [2,3]. Essentially, these systems consist of a baseplate from which regularly spaced microneedles (MNs) made of water-soluble polymers and drug protrude. Once inserted in the skin, the polymeric matrix dissolves in the extracellular fluids of the viable epidermis, enabling drug dissolution and absorption by the rich dermal microcirculation for subsequent systemic distribution [4]. MAPs can be self-applied by users and, because the height of the MNs is lower than 1 mm, they do not reach the blood vessels and nociceptors in deeper layers of the skin, thus avoiding pain and bleeding [5]. Another remarkable advantage for MAPs is that after use, the drug- and needle-free baseplate can be easily peeled off and discarded, avoiding potential needle-stick injuries [6]. All these characteristics make MAPs an appealing platform for the administration of multiple actives to the body, with a wide range of therapeutic applications.

MAPs are often produced using multi-step microfabrication processes in which a blend of the drug and the matrix former polymers are dispersed in a solvent, usually water, and cast into preformed moulds [7,8]. In order to increase drug delivery efficiency, the production of tip-loaded MAPs is desirable, since the drug can be deposited in the skin with minimum drug waste after patch removal, which is particularly relevant for expensive or environmentally contaminant actives. On the other hand, formulations containing the drug in the whole patch (baseplate and MN tips) limit drug delivery efficiency and are useful mostly for cheap, small, water-soluble compounds [9,10]. Moreover, drugs that readily permeate the skin, such as hormones, could be accidentally delivered to other people than the user by simple physical contact. Therefore, the localisation of the drug in the microneedle tips is a highly desirable target, as revealed by recent publications exploring this approach [11–14]. The production of multi-layered MAPs, however, presents several challenges in terms of manufacture, including inadequate MN tip formation due to a limited interaction between the polymer layers, which is exacerbated when hydrophobic drugs are being loaded and the formation of air bubbles during drying [13,15]. This can ultimately be reflected in lack of uniformity, lack of batch-to-batch reproducibility and variable drug content. Finally, the manufacture of MAPs requires up to three days to allow the system to dry, and the polymer excess on the edges of the patches must be removed manually [14,16,17]. Therefore, the development of new methodologies to manufacture MAPs is highly attractive.

One of the crucial features of MAPs is their ability to release drugs in a long-acting fashion [18], which is particularly relevant for long-term treatments. An example of this is the HIV prevention (also known as pre-exposure prophylaxis, PrEP), where MAPs have shown promising results [6,14,19–22]. The human immunodeficiency virus (HIV) still represents an important global health challenge. By the end of 2020, 27.5 million people were accessing antiretroviral (ARV) therapy, meaning that there are 10.2 million people still waiting [23,24]. Importantly, most ARV drugs are currently administered on a daily basis through the oral route in the form of tablets. ARV drugs are also used for HIV PrEP, orally and in the form of local formulations for vaginal and rectal delivery [25–27], subdermal implants [28], and intramuscularly injected long-acting nanosuspensions [29]. However, these lifelong treatments are often associated with sub-optimal adherence and inefficient PrEP protection [30,31]. Therefore, the development of ARV-loaded MAPs is an attractive prospect, since they could overcome many of the disadvantages of currently available treatments, for instance pill fatigue in oral treatments and the use of conventional needles and the need for healthcare infrastructure for injectable formulations.

In this work, we describe for the first time an optimised methodology to prepare tip loaded MAPs loaded with the antiretroviral drug cabotegravir sodium (CAB). A silicone ring insert was prepared using 3D-printed moulds to ensure the localisation of the drug in the MN tips and the efficient formation of a drug-free and uniform baseplate. This approach can be easily transferred to other laboratories for formulation development. Moreover, two manufacture methods, including the use of positive pressures and centrifugation, were explored. Design of experiments (DoE) was used to optimise the MAP formulations, which were evaluated in terms of mechanical properties and *ex vivo* skin deposition in Franz cells using excised full-thickness neonatal porcine skin. Finally, the MAPs were subjected to a pharmacokinetic study in rats to assess their capability of delivering CAB in a long-acting fashion.

2. Materials

Cabotegravir sodium (CAB) of analytical grade was kindly provided by ViiV Healthcare (North Carolina, USA). Poly(vinylpyrrolidone) (PVP k29-32; and PVP k90) was purchased from Ashland (Kidderminster, UK). Poly(vinyl alcohol) (PVA) (9–10 kDa) was obtained from Sigma-Aldrich (Dorset, UK) and. Poly(lactic acid), PLA filament, for the 3D printing of the ring inserts master template was obtained from Ultimaker (Geldermalsen, The Netherlands). Xiameter® RTV-4250-S silicone base and curing agent for the fabrication of the ring inserts were sourced from Notcutt (Surrey, UK). Phosphate buffered saline (PBS) tablets were from Oxoid Ltd, Thermo Fischer Scientific, Massachusetts, USA. Ultrapure water was obtained from an Elga PURELAB DV 25 system (Veolia Water Systems, Dublin, Ireland) and used in all the experiments. All other reagents used in this work were of analytical grade.

3. Methodology

3.1. Microneedle manufacture

3.1.1. Preparation of the drug containing layer

Tip-loaded MAPs were manufactured by micromoulding using silicone moulds with a 16 × 16 needle density (in 0.5 cm^2, interspacing 300 μm), with pyramidal needles of 850 μm in height (250 μm base column, 600 μm pyramidal tip), and 300 μm width at the base. For the drug-containing layer, a blend consisting of 0.84 g of CAB, 1.2 g of a solution made of PVP K90 and PVA (9–10 kDa), both at 40% w/w, (mass ratio 1:1), and 1,000 μL of water. A DAC 150 FVZ SpeedMixer™ (Synergy Devices Limited, High Wycombe, England) was used to homogenise the formulation

(3,000 rpm for 10 min). The resultant blend was poured on top of the silicone moulds and the system was subjected to positive pressure (5 bar for 2.5 min) in a pressure chamber (Airpro AT-10*H*, Taipei, Taiwan). Subsequently, the excess of the blend on the top of the moulds was gently removed with a spatula, and a silicone ring insert (described in Section 3.1.3) was attached to the moulds using PVA (9–10 kDa) 40% w/w as a glue.

3.1.2. Addition of the drug-free baseplate

The baseplate was added using two methodologies involving centrifugation or positive pressure. To this purpose, the baseplate composed of 850 μL 30% w/w PVP k90 aqueous blend was added on top of the pre-formed drug-containing layer. This was followed by either 15 min of centrifugation at 4,332 *g* at 20 °C using an Eppendorf 5804 R centrifuge (Eppendorf, Hamburg, Germany) (formulation code for MAPs prepared by centrifugation: CNT), or 2.5 min at 5 bar in a positive pressure chamber (formulation code PC). After 1.5 days on the bench at room temperature, excess of polymer in the baseplates was trimmed, and the MAPs were left in an oven at 37 °C for further 24 h. MAPs were then stored in a desiccator before characterization.

3.1.3. Ring insert fabrication

Master templates for the ring insert were fabricated using Tinkercad software (Autodesk, Helsinki, Finland) and printed from PLA with an Ultimaker® 3 3D printer (Ultimaker, Geldermalsen, The Netherlands) equipped with Cura® software. For this purpose, 2.85 mm PLA grey filament was used (Ultimaker, Geldermalsen, The Netherlands). The 3D-printing parameters used for the production of the PLA ring templates are presented in Table 1. Xiameter® silicone base was mixed with its curing agent (10:1 w/w), cast into the 3D-printed templates and cured overnight at room temperature to obtain ring inserts with an internal diameter of 18 mm, external diameter of 23 mm, and thickness of 3 mm. Fig. 1 summarises the manufacture method to manufacture the tip-loaded MAPs.

3.2. Microscopical examination

MAPs obtained by the CNT and PC methods were observed under a stereo microscope (Leica EZ4W, Leica Microsystems, Milton Keynes, UK) and the number of MN tips formed was assessed. The experiment was performed in sextuplicate (n = 6), and the results expressed in percentage ± standard deviation.

3.3. MAPs physical testing and insertion capacity

A Texture Analyser (TA.XT2, Stable Micro Systems, Ltd., Haslemere, UK) in compression mode was used to evaluate the MN height reduction. To this purpose, a force of 32 N was applied for 30 s vertically at a downward speed of 1.19 mm/s, representing the human force used for MAPs application, as shown in previous reports [32,33]. MAPs were compressed against a flat aluminium surface and the height of the MNs was measured before and after the test using a stereo microscope (Leica EZ4W, Leica Microsystems, Milton Keynes, UK). The experiment was carried out by quintuplicate (n = 5), and results expressed as percentage height reduction. Insertion studies were carried out using Parafilm M® as a skin-simulant model, which was cut to form eight layers. This method has shown close correlation with results obtained from skin studies [32]. Using the same Texture Analyser set up, insertion was quantified by counting the number of perforations in each Parafilm M® layer when separated and examined under a stereo microscope equipped with two polarizer filters (Leica EZ4W, Leica Microsystems, Milton Keynes, UK).

Table 1
3D-printing parameters used for the production of the PLA templates.

Print Temperature (°C)	Build Plate Temperature (°C)	Print Speed (mm/s)	Layer Height (mm)
200	85	70	0.1

3.4. Determination of MAP and MN tips drug content

Drug content was analysed by dispersing each MAP in 5 mL of water using magnetic stirring until full dissolution of the patch. From this solution, 100 μL were collected into 1.5 mL Eppendorf tubes. Then, 900 μL of acetonitrile (ACN) were added to allow the precipitation of polymer and drug dilution. The tubes were centrifuged at 14,462 *g* for 15 min (Sigma microtube centrifuge SciQuip Ltd, Shropshire, UK), and the supernatant was collected for analysis using high-performance liquid chromatography (HPLC). The same protocol was applied to analyse the drug content in the MN tips, which were carefully harvested in glass vials using a scalpel. Each experiment was carried out in triplicate and the results were expressed as means ± SD.

3.5. Evaluation of skin insertion using optical coherence tomography

MAP insertion in neonatal porcine skin was evaluated using optical coherence tomography (OCT) (EX1301, Michelson Diagnostics Ltd., Kent, UK). To this purpose, both CNT- and PC-MAPs were applied with manual force and OCT images were taken immediately.

3.6. Skin deposition experiments

The skin deposition of CAB MAP was evaluated using excised full-thickness neonatal porcine skin. The skin was obtained from stillborn piglets and excised within 24 h of birth, then packed in an acrylic petri dish and stored in a freezer at −20 °C until use. Before the experiment, the skin was carefully shaved using disposable razors and washed with PBS. The skin was attached to the donor compartment of the Franz cells using cyanoacrylate glue. The CAB MAP applied with manual force for 30 s. The donor compartments were mounted on the Franz cells, and a 20 g stainless-steel cylinder was placed on top of the MAPs to ensure their fixation. PBS (pH 7.4) was used as the release media, and the temperature of the system was kept at 37 ± 1 °C with the aid of a water circulator (Julabo Corio C, Cole Palmer, Vernon Hills, Illinois, USA). The experiment was performed for 24 h with n = 4 for each group. At the endpoint of the study, the skin samples were observed under a stereo microscope and processed as indicated below.

3.6.1. Extraction of drug from skin samples

To extract the drug deposited in the skin, the excess of CAB and polymer on top of the skin was removed by PBS-soaked tissues with mild pressure. Then, the skin samples were cut into small pieces using scissors, placed into a 2 mL Eppendorf tube with 500 μL of water and homogenized for 15 min with 2 metal beads (0.5 cm in diameter) using a TissueLyser® LT (QIAGEN, Manchester, UK) to enable the extraction of the drug. Further homogenisation in the TissueLyser® (15 min) was applied after the addition of another millilitre of ACN. Afterwards, the samples were transferred to a glass vial with 3.5 mL of ACN:H_2O (1:1, v/v), and left in an ultrasonic bath for 2 h. Then, the samples were homogenized using a vortex and 100 μL of the resultant dispersion were mixed with μL of ACN, vortexed again and centrifuged at 14,462 *g* for 10 min

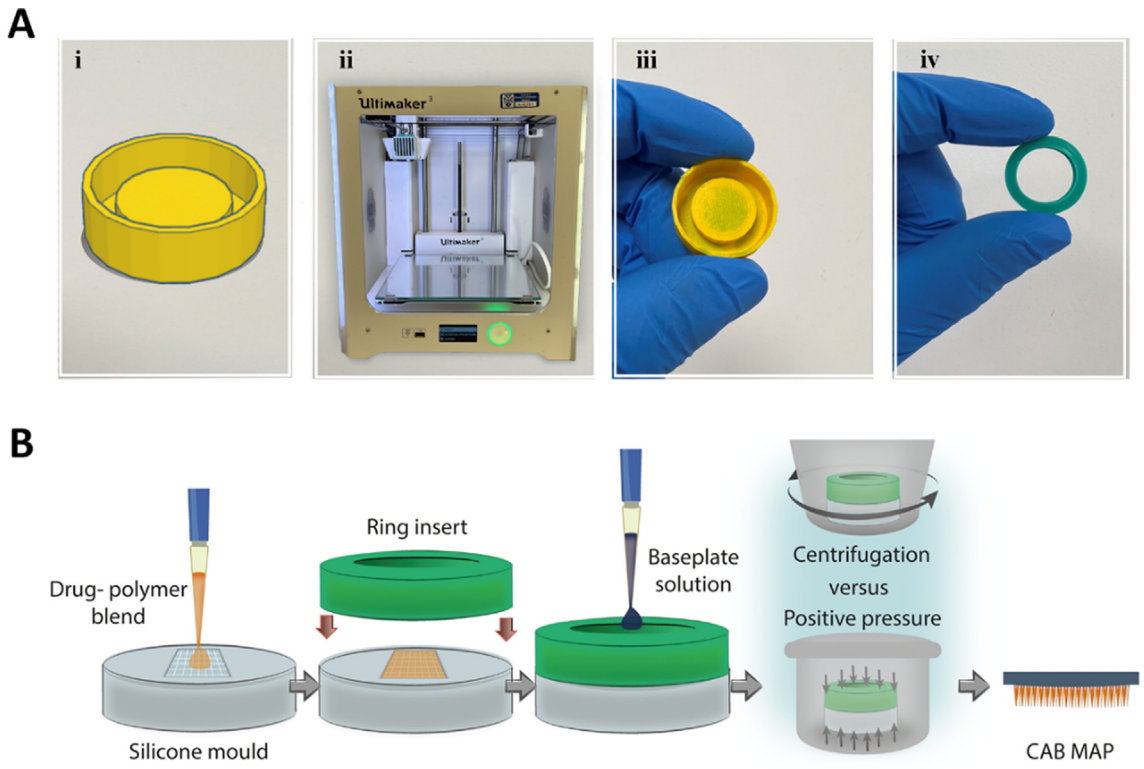

Fig. 1. Summarized methodology used to prepare tip-loaded MAPs using silicone ring inserts. **A**- Manufacture of silicone rings. Design of master templates using CAD Software (**i**), 3D printing of master templates using an Ultimaker® 3D printer (**ii**), picture of a master template for the ring insert printed with PLA (**iii**), picture of a ring insert after silicone curation (**iv**). **B**- Manufacture protocol of bi-layered MAPs using ring inserts. After the ring is fixed and the baseplate solution was added, centrifugation or positive pressure were applied to obtain the final formulations.

(Sigma microtube centrifuge SciQuip Ltd, Shropshire, UK). The CAB content in the supernatant was analysed by HPLC.

3.7. DoE optimization of MAPs manufacture by centrifugation

Aiming to optimize the formulation and evaluate the effect of critical parameters of the centrifugation process on the final formulation, a 2^3 full factorial design was carried out using Design-Expert® Software (StatEase®, Minneapolis, US). The variables assayed were centrifugation force 1,733; 3,032 and 4,332 *g* (corresponding to 2,000; 3,500 and 5,000 rpm in the instrument settings, respectively), and centrifugation time (5, 17.5 and 30 min). To determine the maximum and minimum levels for each parameter, a preliminary set of runs was carried out (data not shown). The minimum centrifugation speed and times were fixed at 2,000 rpm and 5 min, respectively, because below these levels, the adhesion between the baseplate and the first layer were not sufficient to form viable MAPs. For the maximum values, centrifugation times beyond 30 min led to the dissolution of the first layer and its redispersion in the liquid baseplate, leading to incorrect MAP formation. The maximum centrifugation speed was set at 5,000 rpm per the maximum level allowed by the instrument specifications. The response variables chosen were MN formation, MN height reduction and skin deposition, determined in all cases using the correspondent methodologies described above. The variables were assayed in three levels in order to obtain quadratic response surfaces and estimate the characteristics of MAPs based on these independent formulation variables. For each variable, the range of study was chosen according to the results of the initial experiments. Table 2 shows a total of 9 runs was required to complete the study. For avoidance of any biases, the experiments were performed in a randomised order.

Table 2
List of runs for the optimisation of MAP manufacture by centrifugation using design of experiments.

Run	Factor 1: Time (min)	Factor 2: centrifugation force (RPM/*g* force)
1	30	3,500/3,032
2	30	2,000/1,733
3	5	3,500/3,032
4	5	2,000/1,733
5	5	5,000/4,332
6	17.5	3,500/3,032
7	17.5	5,000/4,332
8	30	5,000/4,332
9	17.5	2,000/1,733

3.8. Pharmacokinetic study

The pharmacokinetic experiments were performed in female Sprague Dawley rats of 9–13 weeks of age at the starting point of the study. The animals had access to water and food *ad libitum* throughout the duration of the experiment. The animals were divided in two groups (n = 6), that were treated with CNT MAPs prepared at low centrifugation force (5 min, 1,733 *g*, formulation code: L-CNT MAPs) and high centrifugation force (30 min, 4,332 *g*, formulation code: H-CNT MAPs). Two patches were applied to the back of each rat and blood samples were taken from the tail vein at defined time intervals up to 14 days [14]. The animal studies were carried out with ethical permission from Health Ethical Committee, Hasanuddin University, Indonesia. Plasma samples were obtained by centrifugation of the blood at 1000 *g* and 4 °C for 10 min and stored at −20 °C for extraction and HPLC quantification. In order to extract CAB from plasma samples, 500 μL of

methanol was added to 100 μL of plasma and vortexed for 10 min. The resultant mixture was centrifuged for 15 min at 14,462 *g* at 4 °C. Following this, the clear supernatant was evaporated for 3 h in a fume hood. The dry extract obtained was reconstituted using 100 μL of the mobile phase and analysed using HPLC.

3.8.1. Calculation of pharmacokinetic parameters

The pharmacokinetic curves of the MAPs were constructed by plotting CAB plasma concentrations against time and analyzed using a non-compartmental model. The pharmacokinetic parameters maximum drug concentration (C_{max}), mean residence time (MRT), time of maximum concentration (T_{max}), area under the curve (AUC), and mean half-life ($t_{1/2}$) were calculated using PKSolver software [34].

3.9. Drug quantification

3.9.1. HPLC-UV methodology for in vitro studies

Cabotegravir sodium samples were quantified by using a HPLC-UV method validated for in vitro studies [35]. To this purpose, an Agilent 1200® series system (Agilent Technologies UK Ltd., Stockport, UK) was utilised, Agilent ChemStation® Software B.02.01 were used. Chromatographic separation was possible using an Intersil® ODS-3 C18 column (150 mm × 4.6 mm, 5 μm particle size) at a temperature of 40 °C. The mobile phase was constituted by ACN:trifluoracetic acid (0.1% v/v, pH 2.35) 70:30% v/v, using an isocratic method with UV detection fixed at 257 nm. The run time was 8 min, flow rate 0.8 mL/min, injection volume 40 μL. Stock solution for CAB Na was prepared containing 421.70 μg/mL/CAB Na dissolved in ACN:water (1:1 v/v). Molar equivalence of CAB molecule was considered to develop the method, considering CAB 400 μg/mL = CAB Na 421.70 μg/mL = 9.868×10^{-5} g/mol CAB. Calibration curve was used from 5 − 100 μg/mL.

3.9.2. HPLC bioanalytical method

CAB plasma concentrations were determined by HPLC (Shimadzu Prominence, Shimadzu, Kyoto, Japan) using an Xselect CSH C18 column (3 × 150 mm, particle size: 3.5 μm). A mixture of ACN:trifluoracetic acid (0.1% v/v, pH 2.35) 70:30% v/v was used as the mobile phase. The analysis process was performed using UV detection at 257 nm with flow rate of 1 mL/min and injection volume of 25 μL at room temperature.

3.10. Statistical analysis

To build plots and perform statistical analyses GraphPad Prism© software (version 8.0, GraphPad Software Inc, San Diego, California, USA) was used. To compare more than two cohorts, one-way ANOVA was applied, whereas an unpaired *t*-test was applied when comparing two cohorts. The results were expressed as means ± SD, and in all cases, a p value < 0.05 denoted significance.

4. Results and discussion

4.1. Microneedle formation

Dissolving MAPs loaded with CAB were obtained using both the CNT and PC methods. After the first layer was cast, the MN cavities of the moulds were homogeneously filled, which was visually confirmed by the presence of the white coloured first layer blend forming white dots on the surface of the silicone moulds. The application of the second layer using CNT or PC led to the formation of MAPs with notable differences in terms of uniformity and appearance. As observed in Fig. 2**A**, the amount of MNs formed using the centrifugation method was 99.6 ± 0.5%, whereas the pressure chamber method produced formulations with only 60.8 ± 12.6% of MNs completely formed, with significant differences found between the two groups ($p < 0.0001$, $r^2 = 0.8659$). This agreed with the macroscopical observation of the resultant MAPs, since those prepared using PC showed obvious lack of MN tips and bubbles on the baseplates, which ultimately led to poor adhesion between the first and second layer, and incomplete MN formation as observed in Fig. 2**B**. The same trend was observed when blank (drug free) MAPs were prepared, with the PC method leading to MAPs showing only 69.2 ± 8.1% of the MN formed, against 99.2 ± 1.1% for the blank CNT group. Although positive pressure methods have the potential for large scale MAPs production, one of their main disadvantages is the incorporation of air into the hydrogels that are commonly used to produce the MAPs. Centrifu-

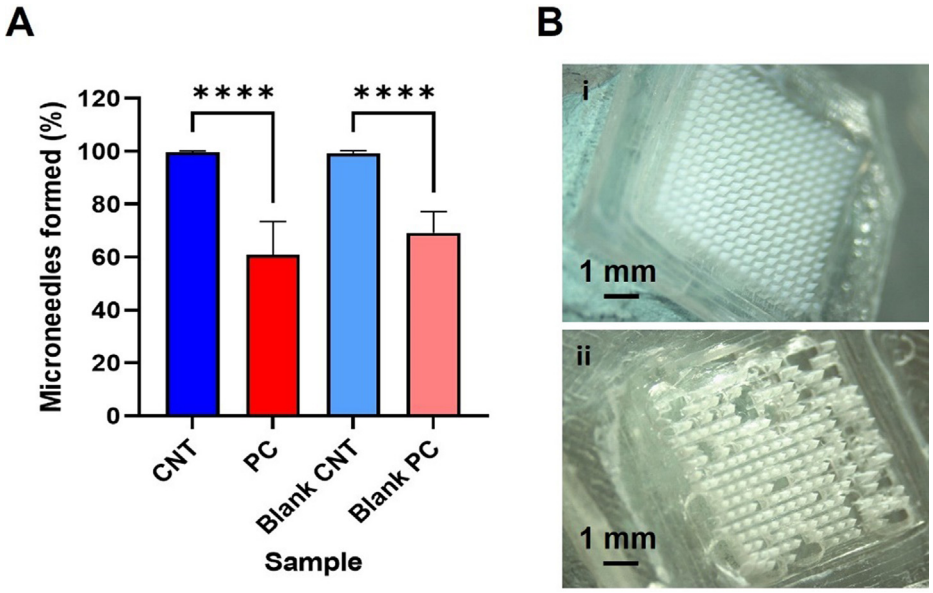

Fig. 2. Microneedle formation in MAPs obtained by centrifugation (CNT) and pressure chamber (PC). (A) Comparative formation of MN tips in drug-loaded MAPs by CNT and PC, and controls obtained using free-drug polymeric blends. (B) Photomicrographs of drug-loaded MAPs obtained from MAPs prepared by CNT (i) and MAPs obtained by PC (ii). **** $p < 0.0001$ ($r^2 = 0.8659$), data expressed as means + SD ($n = 6$).

gation, on the other hand, allowed to obtain highly uniform and bubble-free MAPs.

Centrifugation generates higher forces on the formulation than the PC method. Therefore, the resulting MAPs prepared using CNT methodology shows higher percentage of needle formation. It is important to note that PC methods have been used in the past for the manufacturing of MAPs loaded with nanosuspensions [7,19,20,36,37]. Consequently, the formulation characteristics, such as its viscosity and/or hydrophobicity, can affect the mould filling during the process. Additionally, it is important to note that the PC method will be easier to scale up than centrifugation for industrial manufacturing of MAPs. However, the method described here is intended for formulation development and small batch production in a laboratory set-up. For this purpose, the methodology requires simple equipment that can be found even in humble laboratories. The use of low-cost fused deposition modelling printers allows the production of different rings and adapters for many different MAP designs.

4.2. Mechanical characterisation

The reduction of the MN tips height was determined before and after compression against a flat solid surface. The results can be observed in Fig. 3**A**. The height reduction observed was significantly lower for the CNT MAPs than the PC MAPs, both for the drug loaded and blank formulations ($p < 0.0001$, $r^2 = 0.9410$). This is attributable to the higher MN density that the CNT MAPs have, which allows the distribution of the vertical forces applied among the MN tips. Oppositely, PC MAPs counting with a lower amount of MN tips had a reduced capacity to withstand the mechanical stress. The insertion tests carried out in the skin-simulant Parafilm® model, which has been widely employed after the method was first reported by Larrañeta *et al.* [32]. In this case, the CNT MAPs presented evident differences in the number of holes created in the first and second Parafilm® layers, with both drug-loaded and drug-free formulations following similar patterns. While the CNT MAPs were able to pierce the outermost layers with the vast majority of the MNs, the PC MAPs produced less holes in the Parafilm® layers, given the lower number of microneedles formed. This data indicates that the MN tips themselves were strong enough for penetrating the Parafilm layers, but the hole count was, expectedly, influenced by the number of MN tips formed in the patch.

Despite the lack of pharmacopeial methods for the quality control MAPs, compression and insertion tests can provide valuable information regarding the ability of MAPs to pierce the skin, a key attribute for successful drug delivery *via* the skin. Regarding penetration capacity, the literature shows that MAPs able to perforate two or more Parafilm® layers (equivalent to 252 μm in depth) were able to deliver drugs to the skin, and systemically [14,37,38].

4.3. Drug content in entire MAPs and MN tips

The CAB content in the CNT and PC whole MAPs were 1998.5 0 ± 183.02 μg and 949.85 ± 75.43 μg, respectively, with significant differences found between the two formulations (Fig. 4). This was

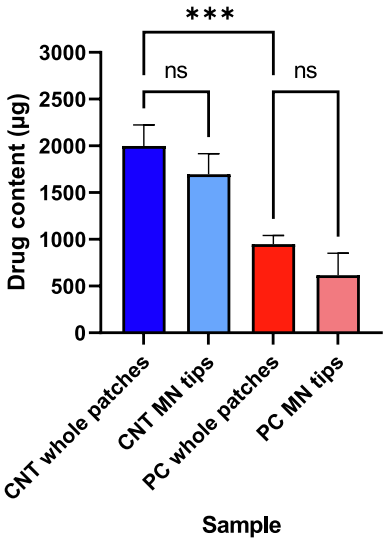

Fig. 4. Drug content of whole MAPs and MN tips. *** $p < 0.0001$, ($r^2 = 0.9197$) one-way ANOVA, ns: not significant, data expressed as means + SD ($n = 3$).

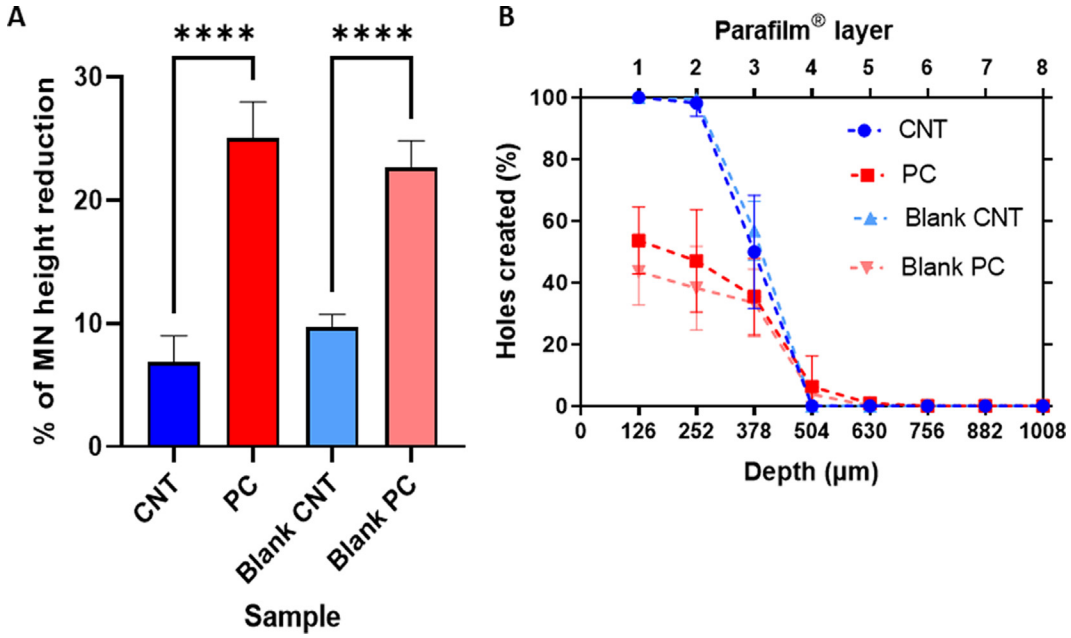

Fig. 3. Mechanical characterisation of MAPs obtained by CNT and PC methods. **A**- Microneedle height reduction after application of vertical force and **B**- MN insertion in the skin simulant Parafilm® model. **** $p < 0.0001$ ($r^2 = 0.9410$) one-way ANOVA, data expressed as mean +/± SD ($n = 5$).

in agreement with the findings of previous sections, where a lower number of MN tips were observed for the formulations obtained by the PC method. CNT methods have been used before to ensure efficient packing of micro- and nanoparticles within MAP tips [39]. On the other hand, the incorporation of air within the still liquid baseplate led to the production of bubbles that were detrimental to the adhesion of the MN tips and the baseplate. Another factor contributing equally for both formulations is the hydrophobicity of the drug, which, likely repels the hydrophilic polymer baseplate. Finally, when comparing the amount of drug in whole patches (i.e., tips and baseplate) with their correspondent MN tips, there were no significant differences found, indicating that the drug was localised in the tips of the MAPs and no back-migration took place.

4.4. Skin deposition experiment

CNT and PC MAPs were able to deposit 488.88 ± 90.31 μg and 261.23 ± 128.89 μg of CAB in the skin respectively, as shown in Fig. 5**A**. The drug delivered to the receptor compartment of the Franz cells was 242.93 ± 158.73 μg and 90.27 ± 13.89 μg for the CNT and PC formulations, respectively (Fig. 5**B**). A significant difference between the two formulations was observed in terms of skin deposition, whereas the amount of drug delivered to the receptor compartment showed clear differences between the two groups, yet with no significant differences. Considering the amount of drug quantified in the MN tips, the percentage deposited in the skin was 28.81% for the CNT MAPs and 39.89% for the PC MAPs. Despite the higher efficiency in drug deposition observed for the PC MAPs, a higher drug amount deposited is more desirable, since this has a greater potential to deliver drug for longer periods, and thus simplify dose regimes [40]. Complementary information regarding the insertion capacity of both formulations to insert in the skin was obtained by using OCT. As shown in Fig. 5**C**, OCT images of the CNT MAPs obtained immediately after MN application revealed a uniform MN tip insertion in the skin, with clear white areas that correspond to the powder drug loaded in the MAPs. Expectedly, the PC MAPs showed discontinued MN tip insertion, with a few MN tips correctly inserted on the left bottom part of the figure, followed by a disruption created by a bubble in the baseplate of the

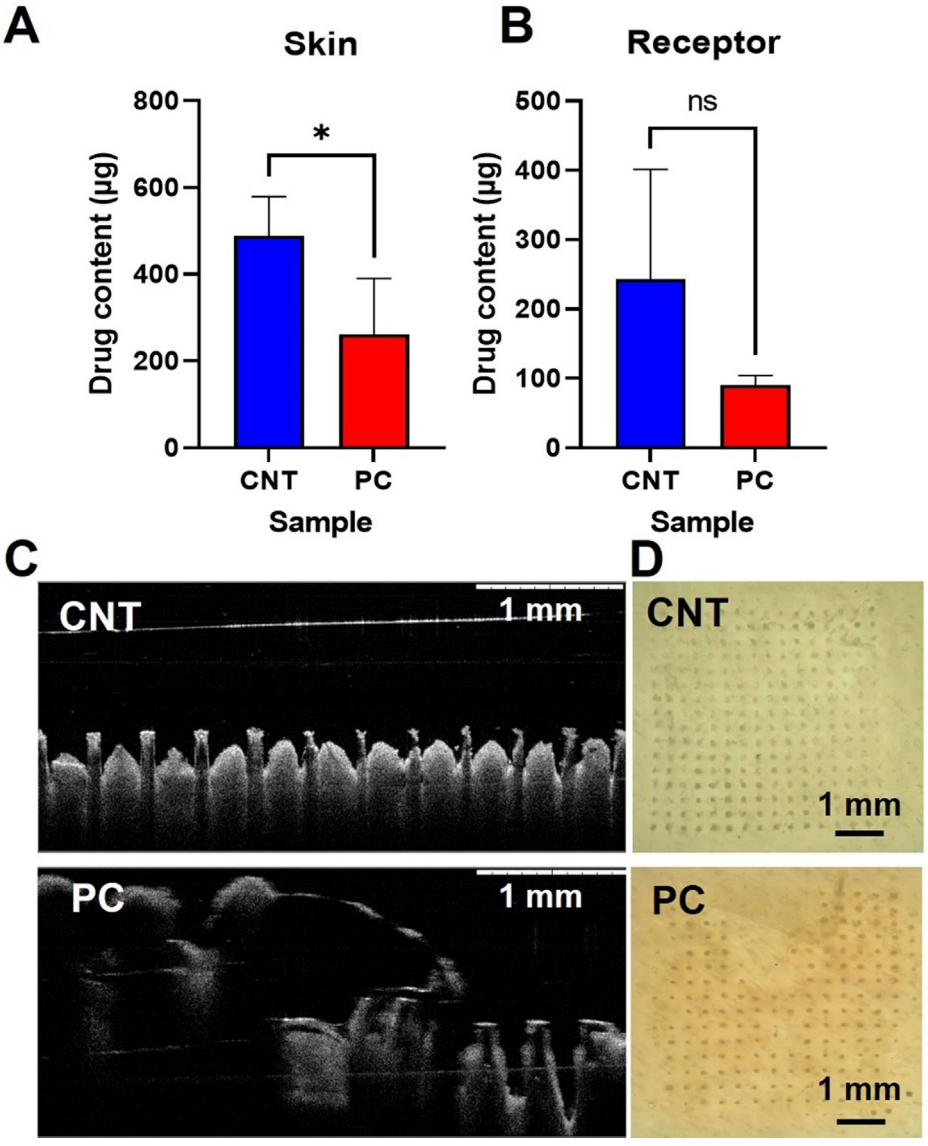

Fig. 5. Drug deposition experiment in excised full-thickness neonatal porcine skin in Franz cells. **A**- Drug quantification in skin; **B**- Drug quantification in the receptor compartment; **C**- Optical coherence tomography taken immediately after MAP skin insertion for CNT-MAPs (CNT) and PC-MAPs (PC); **D**- Optical photomicrograph of the skin after Franz cells experiment (24 h) for CNT-MAPs (CNT) and PC-MAPs (PC), * $p < 0.05$, $r^2 = 0.6063$ one-way ANOVA, ns: not significant, data expressed as means + SD ($n = 4$).

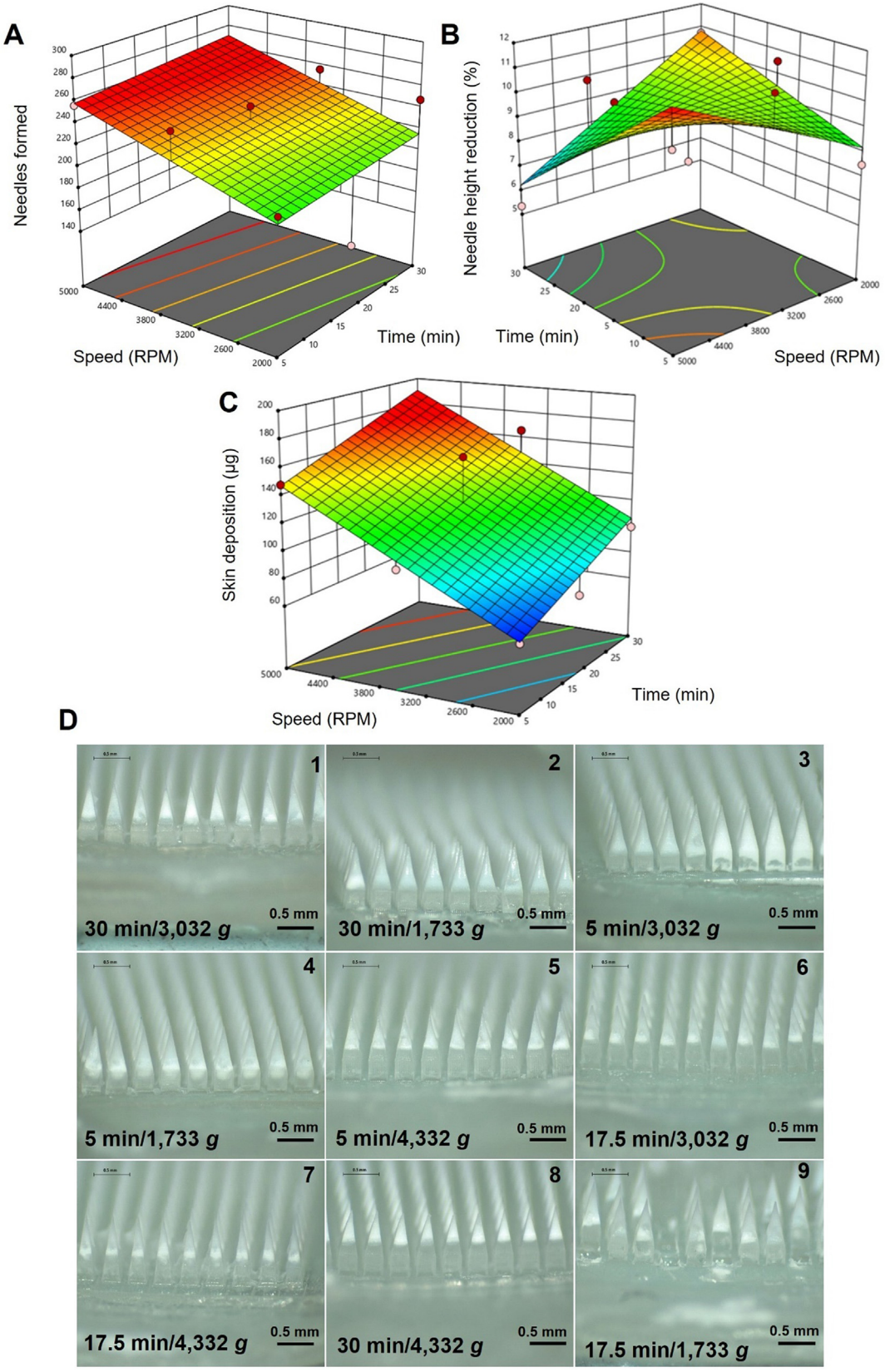

Fig. 6. Optimization of the MAP manufacturing process using centrifugation. The effect of the centrifugation time and force in MN tip formation (**A**), MN tip height reduction (**B**), and skin deposition (**C**). Representative microscopical images of the nine batches corresponding to the optimization process, the centrifugation time and *g* force used for each formulation are expressed in each photomicrograph (**D**).

MAP. Finally, the photomicrographs taken after the 24 h Franz cells experiment and shown in Fig. 5**D** reveals a uniform pattern of holes produced by the insertion of the CNT MAP in the skin. The PC MAPs, on the other hand, had areas with no signs of MN tip insertion, again probably due to the presence of bubbles and incorrect formation of MN tips in these MAPs.

The ability of MAPs to form drug depots in the viable layers of the skin, where it dissolves and slowly diffuses to the dermal microcirculation is a key characteristic of these systems [6]. Franz cell experiments are valuable to assess this capability, since they provide illustration of how much of the drug has been deposited in the skin for long-acting delivery, and how much of the drug permeates across the skin, representing the potential for systemic immediate or sustained delivery. The lower number of MN tips formed in the PC MAPs and their relatively lower drug were in agreement with a poorer performance in the Franz cell experiments, where these formulations deposited significantly lower drug amounts ($p < 0.05$, $r^2 = 0.6063$). Altogether, the results observed in the previous sections demonstrate a deficient capacity of the formulations with baseplates added using positive pressures. Therefore, the CNT MAPs were taken forward to further investigations.

4.5. Optimization of MAP manufacture by centrifugation

Aiming to gain a better understanding of the centrifugation process on the performance of the final formulation, several experiments were carried out varying two independent factors, namely the centrifugation force and time. As responses, the number of needles formed, MN tip height reduction and skin deposition were assessed. Fig. 6**A** displays the trend in MN tip formation at the various *g* forces and times assayed. Here, an increasing trend in MN tip formation was observed when both variables were increased, with a model F-value of 2.29. For instance, a lower centrifugation intensity (low *g* forces and short processing times) led to the formation of 238 microneedle tips, whereas higher energies led to the formation of 256 MN tips, equivalent to 100% of the MN tips available in the silicone moulds. Despite changes observed, the fit statistical analysis produced a *p* value of 0.1828, indicating no significant differences regarding MN tip formation among the processing conditions explored. Regarding MN tip height reduction, the values ranged from 14.71 ± 4.34% to 5.34 ± 1.69% (Fig. 6**B**). However, the statistical analyses showed no significant differences, with a *p* value of 0.2206 (F-value 2.09) indicating a limited relevance of the processing parameter to the percentage of MN tips height reduction, as an indicator of the mechanical strength of these MAPs. On the other hand, the variables assayed presented a considerable impact in the skin deposition within the MAPs assayed, leading to significant differences ($p = 0.0023$, F-value 19.78).

Fig. 6**C** shows an increasing trend in the amount of drug deposited in the skin when increasing both the centrifugation force and time, with values ranging from 62.24 ± 47.13 μg to 174.13 ± 41.10 μg of CAB. The photomicrographs of the nine MAPs resulting from the DoE were observed by the optical microscope and the images are presented in Fig. 6**D** (arranged from 1 to 9 according to the list of runs presented in Table 2. From the observation of these pictures, it is evident that MAPs manufactured at higher centrifugation intensity produced highly uniform MAPs, with clearly identifiable white drug loaded tips, as is the case for formulation 8 (prepared at 4,332 *g*, 30 min). On the other hand, formulation 4, with the lowest centrifugation intensity (1,733 *g*, 5 min), presented a cloudy appearance, with the drug distributed in larger areas of the MN tips. This was in agreement with the data observed in skin deposition response (Fig. 6C), where the formulations produced by at higher centrifugation intensities led to more drug being deposited in the skin. Given the hydrophobic nature of CAB, the drug particles located in the base of the MN tips are less likely to be deposited in the skin. In this case, however, drug concentration in the MN tips led to an enhanced drug deposition. This, in theory, could lead to the formation of drug depots in deeper layers of the skin, closer to the rich skin microcirculation, consequently affecting the pharmacokinetic performance of the formulation. Therefore, the formulations on both extremes in terms of centrifugation intensities, namely high and low (L-CNT MAPs and H-CNT MAPs, respectively), were taken to a pharmacokinetic experiment in rats.

4.6. Pharmacokinetic performance

The pharmacokinetic data obtained for L- and H-CNT MAPs are presented in Fig. 7 and Table 3. The mean plasma concentration profiles indicate a rapid absorption of drug, with detection of CAB in plasma within the first hours of the study. Moreover, both profiles showed similar trends, with plasma levels above the human therapeutic threshold, indicated in the figure with a green dashed line, until day 14. The therapeutic plasma levels that allow 100% of protection against HIV in pre-exposure regimes in humans is 0.664 μg/mL, as reported in the literature, which corresponds to four times the protein-adjusted 90% inhibitory concentration ($4 \times$ PA-IC_{90}) [41]. No significant differences were observed between the two cohorts in terms of AUC, C_{max}, MRT and $T_{1/2}$ values. However, the T_{max} values did show significant differences (L-CNT MAPs: 8 days, H-CNT MAPs: 5 days). This can be possibly attributed to the closeness of the drug depots formed after polymer dissolution to the dermal microvasculature. While the H-CNT MAPs, with the drug more localised in the MN tips, led to a faster peak, the opposite was observed with L-CNT MAPs. Independently of the MAP type, both formulations were able to deliver CAB systemically in a long-acting fashion, maintaining therapeutic plasma levels above the human therapeutic threshold until the endpoint of the study (14 days).

The use of MAPs for HIV PrEP has gained considerable attention over recent years [6]. The HIV epidemic has already claimed 36.3 million lives, and nearly 38 million people were living with HIV in 2020 [23]. Despite a decline in the number of new HIV infections observed, the 90–90–90 target (90% diagnosed, 90% on treatment and 90% virally suppressed) aimed to 2020 by UNAIDS (Joint United Nations Programme on HIV and acquired immunodeficiency syndrome) has still not been achieved [42]. One of the most critical aspects in the fight against HIV is guaranteeing that people can

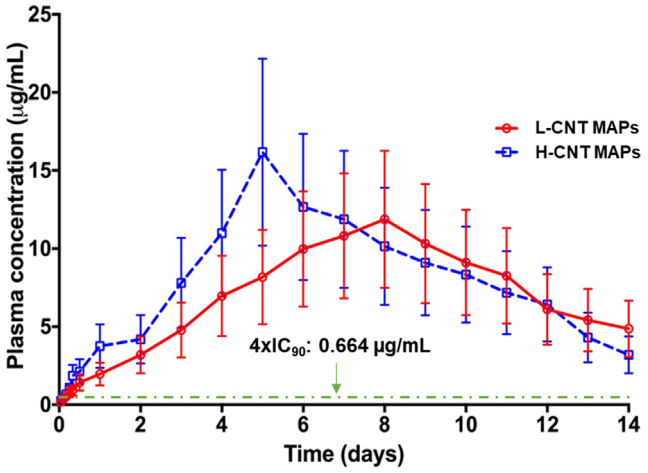

Fig. 7. Pharmacokinetic profiles obtained after the application of L-CNT MAPs and H-CNT MAPs to female Sprague Dawley rats. 4xIC_{90}: indicates the therapeutic plasma concentration in human. Results expressed as means ± SD ($n = 6$).

Table 3
Pharmacokinetic parameters obtained after obtained after the application of L-CNT MAPs and H-CNT MAPs to female Sprague Dawley rats, data expressed as means ± SD (n = 6).

	Formulation	
Parameters	**L-CNT MAPs**	**H-CNT MAPs**
C_{max} (μg/mL)	11.87 ± 3.18	16.18 ± 4.31 ^{ns}
T_{max} (days)	8	5*
AUC_{0-t} (μg/mL.day)	99.66 ± 31.87	114.72 ± 35.82 ^{ns}
AUC_{0-INF} (μg/mL.h)	142.60 ± 35.31	123.83 ± 26.54 ^{ns}
$T_{1/2}$ (days)	6.13 ± 1.74	6.43 ± 1.82 ^{ns}
MRT (days)	12.3 ± 3.31	13.54 ± 3.46 ^{ns}

*Statistically significant difference with the IM formulation, ^{ns}No statistical differences between both assayed cohorts. $T_{1/2}$, CAB half-life; AUC, Area under the curve; MRT, mean residence time.

access ARV drugs, which has demonstrated to improve a patient's life expectancy practically to the same levels as the HIV-negative population in developed countries. The recent approval of an injectable long-acting nanosuspension of CAB free acid (Apretude® from ViiV Healthcare) is considered to be major advancement in HIV PrEP [43,44]. However, the need for hypodermic syringes, trained healthcare professionals, and dedicated infrastructure, might represent a challenge for the correct deployment of the technology in low- and middle-income countries where HIV is more prevalent. In this scenario, the results obtained here are promising, since the user-centric MAPs could deliver these ARVs drugs in a very convenient manner.

5. Conclusions

The work presented here demonstrates the feasibility of a formulation approach using ring inserts to manufacture highly uniform MAPs. The observation of the microneedles confirmed that the vast majority of the MN tips formed correctly using centrifugation and ring inserts. Moreover, consistent formation of uniform baseplates was achieved. The MAPs presented suitable mechanical properties for skin insertion and demonstrated ability to form micro-depots of drug in the viable skin layers. An optimisation experiment revealed that centrifugation parameters had a significant impact in the *ex vivo* skin deposition of the drug. Finally, long-acting drug delivery was observed in the pharmacokinetic study, with therapeutic human plasma levels maintained in rats until the endpoint of the study. The MAPs developed here reveals the potential of this platform, especially in the delivery of long-term dose regimes, including HIV PrEP. The ring inserts developed in this work resulted a viable strategy to produce uniform MAPs in an easy manner at the laboratory scale, and the approach is applicable to other MAPs loading any type of active. Future work includes scalability studies to assess the feasibility of this formulation approach in larger manufacturing set-ups and exploration in greater depth the delivery of antiretroviral drugs, including a combination of actives using MAPs.

CRediT authorship contribution statement

Alejandro J. Paredes: Methodology, Investigation, Formal analysis, Writing – original draft. **Andi Dian Permana:** Methodology, Investigation. **Fabiana Volpe-Zanutto:** Methodology, Investigation. **Muhammad Nur Amir:** Methodology, Investigation. **Lalitkumar K. Vora:** Methodology, Investigation. **Ismaiel A. Tekko:** Methodology, Investigation. **Nima Akhavein:** Writing – review & editing. **Andrew D. Weber:** Writing – review & editing. **Eneko Larrañeta:** Methodology, Investigation, Writing – review & editing. **Ryan F. Donnelly:** Methodology, Investigation, Conceptualization, Supervision, Funding acquisition, Writing – review & editing.

Data availability

Data will be made available on request.

Declaration of Competing Interest

The authors declare the following financial interests/personal relationships which may be considered as potential competing interests: Ryan Donnelly is an inventor of patents that have been licensed to companies developing microneedle-based products and is a paid advisor to companies developing microneedle-based products. The resulting potential conflict of interest has been disclosed and is managed by Queen's University Belfast. The companies had no role in the design of the manuscript, in the collection, analyses or interpretation of the various studies reviewed, in the writing of the manuscript or in the decision to publish.

Acknowledgements

Thanks to ViiV Healthcare for supplying CAB LA injectable formulation and cabotegravir sodium. Via an award to PATH, this project was made possible by the generous support of the American people through the United States Agency for International Development (USAID) through the United States President's Emergency Plan for AIDS Relief (PEPFAR), under the terms of Cooperative Agreement #AID-OAA-A-17-00015. The contents are the responsibility of Queen's University Belfast and do not necessarily reflect the views of USAID, PEPFAR, or the United States government. Also, this work was supported in part by EPSRC grant EP/S028919/1 and Wellcome Trust grant WT094085MA. We would like to thank Biopic3D studio (https://biopic3d.myportfolio.com/) for the design of Fig. 1, and Gina Picco (https://www.instagram.com/ggatmosphere/) for the design of the graphical abstract.

References

[1] X. Chen, H. Xiao, Q. Zhao, X. Xu, Y. Cen, D. Xiao, Research hotspot and trend of microneedles in biomedical field: A bibliometric analysis from 2011 to 2020, Burns 48 (4) (2022) 959–972, https://doi.org/10.1016/j.burns.2022.04.004.
[2] K. Ita, Dissolving microneedles for transdermal drug delivery: Advances and challenges, Biomed. Pharmacother. 93 (2017) 1116–1127, https://doi.org/10.1016/j.biopha.2017.07.019.
[3] Z. Sartawi, C. Blackshields, W. Faisal, Dissolving microneedles: Applications and growing therapeutic potential, J. Control. Release. 348 (2022) 186–205, https://doi.org/10.1016/j.jconrel.2022.05.045.
[4] A.J. Paredes, P.E. McKenna, I.K. Ramöller, Y.A. Naser, F. Volpe-Zanutto, M. Li, M. T.A. Abbate, L. Zhao, C. Zhang, J.M. Abu-Ershaid, X. Dai, R.F. Donnelly, Microarray patches: poking a hole in the challenges faced when eelivering poorly soluble drugs, Adv. Funct. Mater. 31 (1) (2021), https://doi.org/10.1002/adfm.202005792.
[5] T. Waghule, G. Singhvi, S.K. Dubey, M.M. Pandey, G. Gupta, M. Singh, K. Dua, Microneedles: A smart approach and increasing potential for transdermal drug delivery system, Biomed. Pharmacother. 109 (2019) 1249–1258, https://doi.org/10.1016/j.biopha.2018.10.078.
[6] A.J. Paredes, I.K. Ramöller, P.E. McKenna, M.T.A. Abbate, F. Volpe-Zanutto, L.K. Vora, M. Kilbourne-Brook, C. Jarrahian, K. Moffatt, C. Zhang, I.A. Tekko, R.F. Donnelly, Microarray patches: Breaking down the barriers to contraceptive care and HIV prevention for women across the globe, Adv. Drug Deliv. Rev. 173 (2021) 331–348, https://doi.org/10.1016/j.addr.2021.04.002.
[7] A.D. Permana, A.J. Paredes, F. Volpe-Zanutto, Q.K. Anjani, E. Utomo, R.F. Donnelly, Dissolving microneedle-mediated dermal delivery of itraconazole nanocrystals for improved treatment of cutaneous candidiasis, Eur. J. Pharm. Biopharm. 154 (2020) 50–61, https://doi.org/10.1016/j.ejpb.2020.06.025.
[8] F. Volpe-Zanutto, L.T. Ferreira, A.D. Permana, M. Kirkby, A.J. Paredes, L.K. Vora, A. P. Bonfanti, I. Charlie-Silva, C. Raposo, M.C. Figueiredo, I.M.O. Sousa, A. Brisibe, F.T.M. Costa, R.F. Donnelly, M.A. Foglio, Artemether and lumefantrine dissolving microneedle patches with improved pharmacokinetic performance and antimalarial efficacy in mice infected with Plasmodium yoelii, J. Control. Release. 333 (5) (2021) 298–315, https://doi.org/10.1016/j.jconrel.2021.03.036.

[9] P. González-Vázquez, E. Larrañeta, M.T.C. McCrudden, C. Jarrahian, A. Rein-Weston, M. Quintanar-Solares, D. Zehrung, H. McCarthy, A.J. Courtenay, R.F. Donnelly, Transdermal delivery of gentamicin using dissolving microneedle arrays for potential treatment of neonatal sepsis, J. Control. Release. 265 (2017) 30–40, https://doi.org/10.1016/j.jconrel.2017.07.032.

[10] M.T.C. McCrudden, A.Z. Alkilani, C.M. McCrudden, E. McAlister, H.O. McCarthy, A.D. Woolfson, R.F. Donnelly, Design and physicochemical characterisation of novel dissolving polymeric microneedle arrays for transdermal delivery of high dose, low molecular weight drugs, J. Control. Release. 180 (2014) 71–80, https://doi.org/10.1016/j.jconrel.2014.02.007.

[11] YeJin Lee, SeungHyun Park, S.I. Kim, KangJu Lee, WonHyoung Ryu, Rapidly Detachable Microneedles Using Porous Water-Soluble Layer for Ocular Drug Delivery, Adv. Mater. Technol. 5 (2020) 1–10 1901145, https://doi.org/10.1002/admt.201901145.

[12] J.Y. Kim, M.R. Han, Y.H. Kim, S.W. Shin, S.Y. Nam, J.H. Park, Tip-loaded dissolving microneedles for transdermal delivery of donepezil hydrochloride for treatment of Alzheimer's disease, Eur. J. Pharm. Biopharm. 105 (2016) 148–155, https://doi.org/10.1016/j.ejpb.2016.06.006.

[13] A.J. Paredes, F. Volpe-Zanutto, A. Dian Permana, A.J. Murphy, C.J. Picco, L.K. Vora, J.A. Coulter, R.F. Donnelly, Novel tip-loaded dissolving and implantable microneedle array patches for sustained release of finasteride, Int. J. Pharm. (2021), https://doi.org/10.1016/j.ijpharm.2021.120885 120885.

[14] A.J. Paredes, F. Volpe-Zanutto, L.K. Vora, I.A. Tekko, A.D. Permana, C.J. Picco, H. O. McCarthy, R.F. Donnelly, Systemic delivery of tenofovir alafenamide using dissolving and implantable microneedle patches, Mater. Today Bio. 13 (2022), https://doi.org/10.1016/j.mtbio.2022.100217 100217.

[15] A.S. Cordeiro, I.A. Tekko, M.H. Jomaa, L. Vora, E. McAlister, F. Volpe-Zanutto, M. Nethery, P.T. Baine, N. Mitchell, D.W. McNeill, R.F. Donnelly, Two-Photon Polymerisation 3D Printing of Microneedle Array Templates with Versatile Designs: Application in the Development of Polymeric Drug Delivery Systems, Pharm. Res. 37 (2020) 174, https://doi.org/10.1007/s11095-020-02887-9.

[16] M.I. Nasiri, L.K. Vora, J.A. Ershaid, K. Peng, I.A. Tekko, R.F. Donnelly, Nanoemulsion-based dissolving microneedle arrays for enhanced intradermal and transdermal delivery, Drug Deliv. Transl. Res. 12 (2022) 881–896, https://doi.org/10.1007/s13346-021-01107-0.

[17] E. Altuntaş, I.A. Tekko, L.K. Vora, N. Kumar, R. Brodsky, O. Chevallier, E. McAlister, Q. Kurnia Anjani, H.O. McCarthy, R.F. Donnelly, Nestorone nanosuspension-loaded dissolving microneedles array patch: A promising novel approach for "on-demand" hormonal female-controlled peritcoital contraception, Int. J. Pharm. 614 (2022), https://doi.org/10.1016/j.ijpharm.2021.121422 121422.

[18] L.K. Vora, K. Moffatt, I.A. Tekko, A.J. Paredes, F. Volpe-Zanutto, D. Mishra, K.e. Peng, R. Raj Singh Thakur, R.F. Donnelly, Microneedle array systems for long-acting drug delivery, Eur. J. Pharm. Biopharm. 159 (2021) 44–76, https://doi.org/10.1016/j.ejpb.2020.12.006.

[19] I.A. Tekko, L.K. Vora, F. Volpe-Zanutto, K. Moffatt, C. Jarrahian, H.O. McCarthy, R.F. Donnelly, Novel bilayer microarray patch-assisted long-acting micro-depot cabotegravir intradermal delivery for HIV pre-exposure prophylaxis, Adv. Funct. Mater. 32 (9) (2022) 2106999, https://doi.org/10.1002/adfm.202106999.

[20] M.T.C. Mc Crudden, E. Larrañeta, A. Clark, C. Jarrahian, A. Rein-Weston, S. Lachau-Durand, N. Niemeijer, P. Williams, C. Haeck, H.O. McCarthy, D. Zehrung, R.F. Donnelly, Design, formulation and evaluation of novel dissolving microarray patches containing a long-acting rilpivirine nanosuspension, J. Control. Release. 28 (2018) 119–129, https://doi.org/10.1016/j.jconrel.2018.11.002.

[21] F. Volpe-Zanutto, L.K. Vora, I.A. Tekko, P.E. McKenna, A.D. Permana, A.H. Sabri, Q.K. Anjani, H.O. McCarthy, A.J. Paredes, R.F. Donnelly, Hydrogel-forming microarray patches with cyclodextrin drug reservoirs for long-acting delivery of poorly soluble cabotegravir sodium for HIV pre-exposure prophylaxis, J. Control. Release. 348 (2022) 771–785, https://doi.org/10.1016/j.jconrel.2022.06.028.

[22] S. Rojekar, L.K. Vora, I.A. Tekko, F. Volpe-Zanutto, H.O. McCarthy, P.R. Vavia, R.F. Donnelly, Etravirine-loaded dissolving microneedle arrays for long-acting delivery, Eur. J. Pharm. Biopharm. 165 (2021) 41–51, https://doi.org/10.1016/j.ejpb.2021.04.024.

[23] UN Joint Programme on HIV/AIDS (UNAIDS), Global HIV & AIDS statistics - 2020 fact sheet, Glob. HIV Stat. (2020).

[24] hiv.gov, The Global HIV/AIDS Epidemic, Glob. Stat. (2021). https://www.hiv.gov/hiv-basics/overview/data-and-trends/global-statistics (accessed November 22, 2021).

[25] S. Delany-Moretlwe, C. Lombard, D. Baron, L.-G. Bekker, B. Nkala, K. Ahmed, M. Sebe, W. Brumskine, M. Nchabeleng, T. Palanee-Philips, J. Ntshangase, S. Sibiya, E. Smith, R. Panchia, L. Myer, J.L. Schwartz, M. Marzinke, L. Morris, E.R. Brown, G.F. Doncel, G. Gray, H. Rees, Tenofovir 1% vaginal gel for prevention of HIV-1 infection in women in South Africa (FACTS-001): a phase 3, randomised, double-blind, placebo-controlled trial., Lancet, Infect. Dis. 18 (2018) 1241–1250, https://doi.org/10.1016/S1473-3099(18)30428-6.

[26] Q. Abdool Karim, S.S. Abdool Karim, J.A. Frohlich, A.C. Grobler, C. Baxter, L.E. Mansoor, A.B.M. Kharsany, S. Sibeko, K.P. Mlisana, Z. Omar, T.N. Gengiah, S. Maarschalk, N. Arulappan, M. Mlotshwa, L. Morris, D. Taylor, Effectiveness and Safety of Tenofovir Gel, an Antiretroviral Microbicide, for the Prevention of HIV Infection in Women, Science 329 (5996) (2010) 1168–1174, https://doi.org/10.1126/science.1193748.

[27] M.J. Keller, L. Wood, J.M. Billingsley, L.L. Ray, J. Goymer, S. Sinclair, A.P. McGinn, M.A. Marzinke, B. Frank, S. Srinivasan, C. Liu, J.M. Atrio, L. Espinoza, N. Mugo, H. M.L. Spiegel, P.L. Anderson, D.N. Fredricks, C.W. Hendrix, J. Marrazzo, S.E. Bosinger, B.C. Herold, Tenofovir disoproxil fumarate intravaginal ring for HIV pre-exposure prophylaxis in sexually active women: a phase 1, single-blind, randomised, controlled trial, Lancet HIV. 6 (2019) e498–e508. https://doi.org/10.1016/S2352-3018(19)30145-6.

[28] C. Flexner, D.L. Thomas, S. Swindells, Creating demand for long-acting formulations for the treatment and prevention of HIV, tuberculosis, and viral hepatitis, Curr. Opin. HIV AIDS. 14 (2019) 13–20, https://doi.org/10.1097/COH.0000000000000510.

[29] J. Abbasi, Long-acting Cabotegravir Shot Prevents HIV among Women, JAMA - J. Am. Med. Assoc. 324 (2020) 2247, https://doi.org/10.1001/jama.2020.23330.

[30] UNAIDS, Prevention Gap Report, Unaids. (2016). http://www.unaids.org/sites/default/files/media_asset/2016-prevention-gap-report_en.pdf (accessed November 22, 2021).

[31] K.R. Claborn, E. Meier, M.B. Miller, T.R. Leffingwell, A systematic review of treatment fatigue among HIV-infected patients prescribed antiretroviral therapy, Psychol, Health Med. 20 (2015) 255–265, https://doi.org/10.1080/13548506.2014.945601.

[32] E. Larrañeta, J. Moore, E.M. Vicente-Pérez, P. González-Vázquez, R. Lutton, A.D. Woolfson, R.F. Donnelly, A proposed model membrane and test method for microneedle insertion studies, Int. J. Pharm. 472 (2014) 65–73, https://doi.org/10.1016/j.ijpharm.2014.05.042.

[33] I.K. Ramöller, I.A. Tekko, H.O. McCarthy, R.F. Donnelly, Rapidly dissolving bilayer microneedle arrays – A minimally invasive transdermal drug delivery system for vitamin B12, Int. J. Pharm. 566 (2019) 299–306, https://doi.org/10.1016/j.ijpharm.2019.05.066.

[34] Y. Zhang, M. Huo, J. Zhou, S. Xie, PKSolver: An add-in program for pharmacokinetic and pharmacodynamic data analysis in Microsoft Excel, Comput. Methods Programs Biomed. 99 (2010) 306–314, https://doi.org/10.1016/j.cmpb.2010.01.007.

[35] FDA, Q2B Validation of Analytical Procedures: Methodology, Methodology 60 (40) (1995) 11260–11262. https://www.fda.gov/regulatory-information/search-fda-guidance-documents/q2b-validation-analytical-procedures-methodology.

[36] M.T.C. Mc Crudden, E. Larrañeta, A. Clark, C. Jarrahian, A. Rein-Weston, B. Creelman, Y. Moyo, S. Lachau-Durand, N. Niemeijer, P. Williams, H.O. McCarthy, D. Zehrung, R.F. Donnelly, Design, formulation, and evaluation of novel dissolving microarray patches containing rilpivirine for intravaginal delivery, Adv. Healthc. Mater. 8 (2019) 1801510, https://doi.org/10.1002/adhm.201801510.

[37] A.D. Permana, A.J. Paredes, F.V. Zanutto, M.N. Amir, I. Ismail, M.A. Bahar, Sumarheni, S.D. Palma, R.F. Donnelly, Albendazole nanocrystal-based dissolving microneedles with improved pharmacokinetic performance for enhanced treatment of cystic echinococcosis, ACS Appl. Mater. Interfaces. 13 (32) (2021) 38745–38760, https://doi.org/10.1021/acsami.1c11179.

[38] L. Lopez-Vidal, J. Pablo Real, D. Andrés Real, N. Camacho, M.J. Kogan, A.J. Paredes, S.D. Palma, Nanocrystal-based 3D-printed tablets: Semi-solid extrusion using melting solidification printing process (MESO-PP) for oral administration of poorly soluble drugs, Int. J. Pharm. 611 (2021), https://doi.org/10.1016/j.ijpharm.2021.121311 121311.

[39] L.K. Vora, R.F. Donnelly, E. Larrañeta, P. González-Vázquez, R.R.S. Thakur, P.R. Vavia, Novel bilayer dissolving microneedle arrays with concentrated PLGA nano-microparticles for targeted intradermal delivery: Proof of concept, J. Control. Release. 265 (2017) 93–101, https://doi.org/10.1016/j.jconrel.2017.10.005.

[40] W. Li, J. Tang, R.N. Terry, S. Li, A. Brunie, R.L. Callahan, R.K. Noel, C.A. Rodríguez, S.P. Schwendeman, M.R. Prausnitz, Long-acting reversible contraception by effervescent microneedle patch, Sci. Adv. 5 (2019) eaaw814, https://doi.org/10.1126/sciadv.aaw8145.

[41] C. Trezza, S.L. Ford, W. Spreen, R. Pan, S. Piscitelli, Formulation and pharmacology of long-acting cabotegravir, Curr. Opin. HIV AIDS. 10 (2015) 239–245, https://doi.org/10.1097/COH.0000000000000168.

[42] UN Joint Programme on HIV/AIDS (UNAIDS), 90–90–90: good progress, but the world is off-track for hitting the 2020 targets, (2020). https://www.unaids.org/en/resources/presscentre/featurestories/2020/september/20200921_90-90-90 (accessed March 15, 2021).

[43] M.B. McGuckin, J. Wang, R. Ghanma, N. Qin, S.D. Palma, R.F. Donnelly, A.J. Paredes, Nanocrystals as a master key to deliver hydrophobic drugs via multiple administration routes, J. Control. Release. 345 (2022) 334–353, https://doi.org/10.1016/j.jconrel.2022.03.012.

[44] Food and Drug Administration, FDA approves first injectable treatment for HIV pre-exposure prevention, FDA News Release. (2021). https://www.fda.gov/news-events/press-announcements/fda-approves-first-injectable-treatment-hiv-pre-exposure-prevention (accessed June 16, 2022).